The Astrophysical Journal Letters, 947:L16 (6pp), 2023 April 10 https://doi.org/10.3847/2041-8213/acca1f

The Game of Life on a Magnetar Crust: From Gamma-Ray Flares to FRBs

S. K. Lander
Physics, Faculty of Science, University of East Anglia, Norwich, NR4 7TJ, UK; samuel.lander@uea.ac.uk
Received 2023 March 14; revised 2023 March 30; accepted 2023 April 4; published 2023 April 18

Abstract

This Letter presents a model to unify the diverse range of magnetar activity, through the building and release of elastic stress from the crust. A cellular automaton drives both local and global yielding of the crust, leading to braiding of coronal loops and energy release. The model behaves like a real magnetar in many ways: giant flares and small bursts both occur, as well as periods of quiescence whose typical duration is either $\lesssim$1 yr or $\sim$10–30 yr. The burst energy distribution broadly follows an earthquake-like power law over the energy range 10^{40}–10^{45} erg. The local nature of coronal loops allows for the possibility of high-energy and fast radio bursts from the same magnetar. Within this paradigm, magnetar observations can be used to constrain the poorly understood mechanical properties of the neutron-star crust.

Unified Astronomy Thesaurus concepts: Neutron stars (1108); X-ray bursts (1814); Radio bursts (1339); Magnetars (992)

1. Introduction

Magnetars, a class of restless neutron stars characterized by energetic outbursts, drive a wide range of astrophysical phenomena: from short X-ray bursts of $\lesssim 10^{41}$ erg, through storms of bursts and prolonged intermediate events, up to rare giant γ-ray flares of 10^{44}–10^{46} erg, among the most violent events in the universe (Turolla et al. 2015; Kaspi & Beloborodov 2017). Very recently, observations (Bochenek et al. 2020; CHIME/FRB Collaboration et al. 2020; Mereghetti et al. 2020; Li et al. 2021; Ridnaia et al. 2021) have shown us that magnetars are also the central engines for at least some fast radio bursts (FRBs), that some short γ-ray bursts are the result of giant flares from extragalactic magnetars (Burns et al. 2021), and that certain ultralong-period radio emitters may be old magnetars (Beniamini et al. 2022; Caleb et al. 2022; Hurley-Walker et al. 2022). In all its activity, the magnetar's solid crust plays a key role: it stores an enormous amount of energy in the form of elastic stress τ built up as the intense internal magnetic field $\boldsymbol{B}$ evolves; seismic events then release some of this energy into the corona, ultimately leading to the activity we observe (Ruderman 1991; Thompson & Duncan 1995; Perna & Pons 2011; Lander et al. 2015; Dehman et al. 2020).

Compared with the detailed quantitative simulations of crustal magnetic field evolution (Pons & Viganò 2019; Gourgouliatos et al. 2022), our modeling of how the crust releases elastic energy is rudimentary, and faces conceptual challenges (Thompson et al. 2017). Furthermore, even the qualitative picture of magnetar activity is disjointed, with, e.g., short bursts and giant flares generally treated as being of different physical origin, impeding any attempts to probe the underlying crustal physics. Here, by contrast, we show how the full spectrum of magnetar activity can be interpreted by taking a new approach: a single, physically motivated model of the crust as a cellular automaton that drives coronal activity and thus the observed bursting behavior.

2. Model

2.1. Crustal Failure

The outer crust of a magnetar, with a density $\rho < 4 \times 10^{11}\,\mathrm{g\,cm^{-3}}$, is relatively weak and will be partially molten for younger stars; although it may be the source of weak bursts (Younes et al. 2022) we neglect its effect here, and concentrate on the more universal role of the inner crust, an immensely strong crystalline structure that resists and responds elastically to any imposed force, until it reaches its elastic yield stress $\tau_{\rm el}$. When the crust eventually yields, the high pressure inhibits the formation and propagation of voids through the crustal lattice, so instead of a brittle fracture the crust is expected to flow plastically (Jones 2003), releasing elastic energy.[1]

To study crustal failure quantitatively, we will first need profiles of the mass and charge density ρ, ρ_e and composition throughout the crust. These are found by solving the relativistic stellar structure equations together with the SLy4 equation of state, as in Lander & Gourgouliatos (2019). Fixing the mass at $1.4M_\odot$ gives us a model of radius 11.7 km, whose inner crust is 550 m thick, which we adopt throughout this Letter.

To estimate the free energy reservoir of the crust, we evaluate the formula for $\tau_{\rm el}$ from Chugunov & Horowitz (2010) and volume-integrate it over the inner crust to find a maximum elastic energy $E_{\rm el} \sim \int \tau_{\rm el}\, dV = 4\pi \int \tau_{\rm el}(r) r^2 dr \approx 10^{47}$ erg. The energy of the magnetic field threading the crust is comparable with $E_{\rm el}$; if this is also tapped during crustal failure, the total energy reservoir becomes $\sim 2 \times 10^{47}$ erg. This is a factor of $\sim$10 greater than the most powerful known giant flare (Palmer et al. 2005); crustal energy alone is therefore able, in principle, to explain all magnetar activity observed to date.

Crustal yielding is an essential part of the magnetar paradigm, as it drives the transfer of energy, via the motion of embedded coronal field footpoints, out to the corona, from where it is released in the activity we observe (Lyutikov 2006). A major challenge in neutron-star physics is how yielding occurs; microscopic molecular-dynamics simulations exhibit

[1] Note, however, that in the model of Thompson et al. (2017) narrow crack-like plastic features develop.

collective local failure (Horowitz & Kadau 2009), but if every small group of crustal ions were to yield as soon as $\tau = \tau_{\rm el}$, all resultant bursts would be undetectably small. Equally, the crust's stress distribution is likely to be highly anisotropic, with regions where $\tau \approx \tau_{\rm el}$ and others with $\tau \ll \tau_{\rm el}$, so it is energetically disfavored for every local failure to grow into a global one. Furthermore, this would lead to a scenario, contradicted by observations, where a magnetar would be unable to produce repeated small bursts. An additional piece of physics must, therefore, set the characteristic lengthscale for crustal failure.

2.2. The Crust as an Array of Cells

First-principles macroscopic simulations of crustal failure are currently out of reach, but there are many clues to guide us to the origin of magnetar activity. Observationally, numerous studies have shown how bursting activity appears to come from relatively small patches of the crust (Palmer 1999; Younes et al. 2022), often at locations across the stellar surface (Scholz & Kaspi 2011; Younes et al. 2020), meaning that crustal failure must often be a local phenomenon. Both high-energy bursts (Cheng et al. 1996) and FRBs (Wadiasingh & Timokhin 2019) exhibit a power-law distribution of number versus energy, like that of earthquakes (Bak et al. 2002). From the theory side, 3D numerical evolutions of the crustal magnetic field show the development of $\sim$1 km^2 patches with strong B_ϕ (Gourgouliatos et al. 2016; Igoshev et al. 2021); this significant change from the initial B induces high stress (Lander & Gourgouliatos 2019), and so elastic failure is likely to occur within such patches, but not necessarily spread beyond them. On the other hand, a crust-powered giant flare requires a larger-scale failure, to explain the amount of energy released and how much quieter the star becomes afterwards; the model must therefore also allow for this possibility.

Guided by these considerations, we split the inner crust into an array of semiautonomous cells with fixed boundaries, each of surface area 1 km^2. To fix the cell depth, we note that since $\tau_{\rm el}$ increases by a factor of $\sim$1000 from the top to the base of the inner crust, we do not expect every local failure of a cell to propagate to the full 550 m depth of the inner crust. Instead we fix the cell depth at 200 m, over which $\tau_{\rm el}$ varies by less than 1 order of magnitude, and assume that the crystalline structure in such a cell always fails collectively. As a result, we can ignore variations of the stress within a cell and assume it is given by a single spatially constant τ that evolves with time. This evolution is dependent on other parameters (see Equation (3)), so for consistency we therefore assume there is no spatial variation in *any* physical quantity within a cell; we use the value of each from the base of the cell. Physical quantities do, however, vary from cell to cell across the crust.

When a cell's stress exceeds the elastic yield value, $\tau > \tau_{\rm el}$, only a fraction of it is expected to be relieved in the ensuing plastic flow (Lander & Gourgouliatos 2019); if we assume for definiteness a 10% reduction from $\tau_{\rm el}$, the corresponding energy release is 3×10^{40} erg—similar to a fairly powerful short X-ray burst, and providing a sanity check of the cell model.

We regard a cell's stress as being sourced by the magnetic field $\boldsymbol{B}$ alone and define a scalar stress $\tau \equiv B^2/4\pi$. Neglecting the effect of ohmic decay—reasonable for young magnetars (Pons & Viganò 2019)—the evolution of $\boldsymbol{B}$ in a crust stressed beyond $\tau_{\rm el}$ is dictated by an interplay of Hall drift and advection due to plastic flow $\boldsymbol{v}_{\rm pl}$:

$$\frac{\partial \boldsymbol{B}}{\partial t} = -\nabla \times \left[\frac{c}{4\pi \rho_e} (\nabla \times \boldsymbol{B}) \times \boldsymbol{B} \right] + \nabla \times (\boldsymbol{v}_{\rm pl} \times \boldsymbol{B}). \quad (1)$$

We model the crust as a Bingham plastic: below $\tau_{\rm el}$ its response to stress is purely elastic, with $\boldsymbol{v}_{\rm pl} = 0$ and only the Hall drift term present in (1), while above $\tau_{\rm el}$ the crust behaves as a viscoplastic with flow velocity $v_{\rm pl} \propto (\tau - \tau_{\rm el})$. Specifically, we use a scalar version of the slow viscous-flow model of Lander & Gourgouliatos (2019), produced by replacing spatial derivatives $\nabla \to 1/L$ (where L is a characteristic lengthscale):

$$v_{\rm pl} = \frac{L}{\nu}(\tau - \tau_{\rm el}), \quad (2)$$

where ν is the viscosity of crustal matter in its plastic phase. Now, from (1) we can derive an approximate scalar equation for τ, by using the identity $\partial B^2/\partial t = 2\boldsymbol{B} \cdot \partial \boldsymbol{B}/\partial t$, and eliminating B, $v_{\rm pl}$ using (2) and the relation $\tau = B^2/4\pi$:

$$\frac{d\tau}{dt} = \frac{c\tau^{3/2}}{\pi^{1/2}\rho_e L^2} - \frac{2\tau(\tau - \tau_{\rm el})}{\nu}, \quad (3)$$

where we have swapped the signs on the two right-hand-side terms to reflect the tendency of Hall drift to increase τ and plastic flow to reduce it.

Simulations (Lander & Gourgouliatos 2019; Gourgouliatos & Lander 2021) show that stresses substantially higher than $\tau_{\rm el}$ may form before plastic flow has a chance to relieve them; to mimic this we model a cell's response as elastic and allow τ to grow under the Hall effect, until it reaches a critical value $\tau = 1.1\tau_{\rm el}$. At this point failure occurs and in principle there will be an interplay between the Hall and plastic terms. To understand this, let us use (3) to estimate characteristic timescales $\mathrm{t}_{\rm Hall}$, $\mathrm{t}_{\rm pl}$ for the evolution of stress under Hall drift and plastic flow:

$$\mathrm{t}_{\rm Hall} = \frac{\pi^{1/2}\rho_e L^2}{c\tau^{1/2}} \approx 800\ \mathrm{yr}, \quad \mathrm{t}_{\rm pl} = \frac{\nu}{2(\tau - \tau_{\rm el})} \approx 9\ \mathrm{yr}, \quad (4)$$

using typical values: $L = 200$ m, $\tau = 1.1\tau_{\rm el}$, $\rho_e = 1.4 \times 10^{26}$ esu cm^{-3}, and $\nu = 10^{36}$ poise. The Hall effect is always active, but may reasonably be neglected during the plastic phase, since $\mathrm{t}_{\rm pl} \ll \mathrm{t}_{\rm Hall}$. During the elastic phase, only the Hall effect operates. Therefore, we model a single cell's evolution as alternating phases of growth of τ until the value $1.1\tau_{\rm el}$ is reached, followed by a reduction of τ down to $\tau_{\rm el}$ under the action of plastic flow.[2]

Time-integrating (3), we find closed-form expressions $\tau = \tau(t, t_{\rm swap})$ for both the Hall and plastic phases, where $t_{\rm swap}$ is the time at which the current phase began. The Hall phase takes 75 yr, and the plastic phase $\sim$1–5 yr—somewhat shorter than the timescale estimates of (4), since here τ is only reduced by 10%.

The crust's temperature T has a minimum "ambient" value $T_{\rm amb}$ defined at the start of each simulation. We wish to consider a range for $T_{\rm amb}$ that encompasses all neutron stars that might plausibly display bursting activity, from young magnetars whose high surface T appear to require a heat source in the crust (Beloborodov & Li 2016), to old sources ($>10^4$ yr)

[2] More precisely, since $d\tau/dt \to 0$ as $\tau \to \tau_{\rm el}$, the plastic phase is ended at $\tau = 1.0001\tau_{\rm el}$.

that have experienced no heating since birth. These considerations lead us to adopt, based on the cooling evolutions of Ho et al. (2012), the range[3] $T_{\rm amb,9} \equiv T_{\rm amb}/(10^9\ {\rm K}) = 0.05$–$0.5$. Next, $\boldsymbol{v}_{\rm pl}$ causes heating at rate $Q_{\rm pl}$, which we model using an approximation to Equation (21) from Li et al. (2016):

$$\frac{dT}{dt} = \frac{Q_{\rm pl}}{C_V} \sim \frac{B^2}{4\pi C_V}\frac{v_{\rm pl}}{L} = \frac{1}{\nu C_V}\tau(\tau - \tau_{\rm el}), \tag{5}$$

integrating from $T = T_{\rm amb}$ at the start of the plastic phase, and where C_V is the specific heat capacity. 60% of this heat is assumed to stay in the cell and the rest to diffuse to its surroundings, to mimic the effect of thermal conductivity. Once the plastic phase ends, $T \to T_{\rm amb}$ linearly over a timescale $\approx C_V T/Q_\nu \approx 13$ yr (setting $T_9 = 1$ for the plastically heated cell, and using values for C_V and neutrino emissivity Q_ν from Gnedin et al. 2001, evaluated at the base of the cell as usual).

Finally, we need an expression for ν. Since this is unknown from first principles, numerical experimentation has been required to understand the range of plausible values that produce an interplay between Hall drift and plastic flow, and therefore allow for magnetar activity (Lander 2016). Following Lander & Gourgouliatos (2019), the density dependence of ν is taken to be the same as for $\tau_{\rm el}$. The T dependence of viscous fluids is often approximated by the Andrade equation (Andrade 1934), where $\nu \propto e^{1/T}$. Modifying this to avoid the divergent behavior (problematic for a solid) as $T \to 0$, and adjusting constants to match previous work (Lander & Gourgouliatos 2019; Gourgouliatos & Lander 2021; Kojima et al. 2021), we arrive at the phenomenological relation

$$\nu(\rho, T) = 5 \times 10^5 \tau_{\rm el}(\rho) e^{5/(1+T_9)}\ {\rm poise}, \tag{6}$$

giving a possible range $10^{34} \lesssim \nu \lesssim 10^{36}$ poise for a cell. Heating reduces ν, affecting the crust's activity in two opposing ways: on the one hand it increases $v_{\rm pl}$ and the rate of coronal twisting; on the other hand it shortens the plastic phase and reduces the chances of several plastic cells having time to join up into a cluster, which in turn makes future deep failures and giant flares less likely. Any other relation for ν of the same order of magnitude, and reducing with T, would lead to broadly similar results.

2.3. Cellular Automaton

Having described the physics of a single cell, we need to understand how they interact. We assume a cell's behavior only affects its four von Neumann neighbors (i.e., those with whom it shares an edge). It is well known that complex physics can arise from simple cellular automata (Von Neumann & Burks 1966; Berlekamp et al. 2004). At the same time, these rules need to be linked to underlying physics as rigorously as possible to have any predictive power, and results cannot be artifacts of a fine-tuned model, but should be robust and generic: self-organized criticality (SOC; Katz 1986; Bak et al. 1988). There is evidence that both X-ray bursts and FRBs are driven by the same SOC process (Wei et al. 2021), motivating the present study.

Crustal magnetic field lines thread multiple cells and are dragged around locally by $\boldsymbol{v}_{\rm pl}$ in a cell. This exerts a shearing force on its neighbors, but cannot cause them all to fail—otherwise every localized $\boldsymbol{v}_{\rm pl}$ could quickly propagate across the entire crust. Instead, we encode this effect through a cell rule: a cell in its elastic phase normally switches to its plastic phase at $\tau = 1.1\tau_{\rm el}$, but for every plastic neighbor, the cell's yield stress is lowered by $0.025\tau_{\rm el}$; nearby plastic flow thus *hastens*, rather than triggers, a cell's failure. This is the key rule that leads to SOC-like behavior of the model. A contiguous cluster of plastic cells is regarded as a single physical entity, with $\boldsymbol{v}_{\rm pl}$ circulating across the entire cluster with some average velocity $\bar{v}_{\rm pl}$.

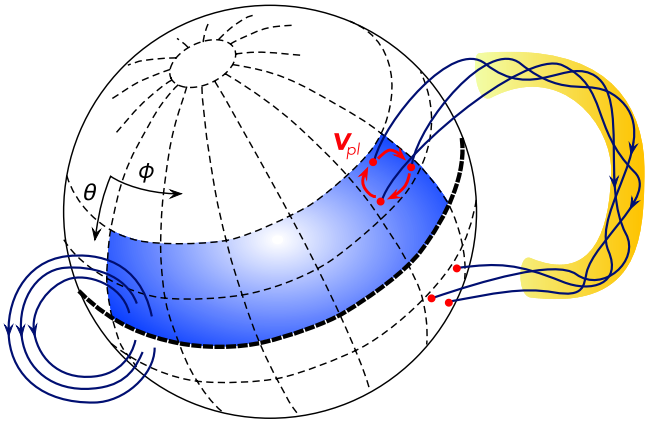

Figure 1. The magnetar crust as an array of cells. The left-hand bunch of coronal field lines are untwisted, embedded in a static cell in its elastic phase. The right-hand bunch are braided by a plastic flow $\boldsymbol{v}_{\rm pl}$ circulating around a cell whose elastic yield stress has been exceeded.

Shallow failures, down to the base of the cells, do not release enough energy to explain larger magnetar events, so the deeper crust—which will also be close to its $\tau_{\rm el}$—must also fail sometimes. Our criterion for this to occur is that the cell itself, and at least three neighbors, must all be in a plastic phase simultaneously. Such a "deep" failure below a cell releases all stored elastic energy in that region, down to the crust–core boundary. Thereafter we assume $\tau = 0$ for that cell (replenishing τ back to $\tau_{\rm el}$ through the entire inner crust would take substantially longer than the previous estimate (4) of $t_{\rm Hall} \approx 800$ yr); in this way, magnetar crustal dynamics are analogous to forest-fire models (Drossel & Schwabl 1992).

2.4. Corona

The most readily induced kind of plastic flow satisfies $\nabla \cdot \boldsymbol{v}_{\rm pl} = 0$ and has no radial component (Lander 2016). Restricting $\boldsymbol{v}_{\rm pl}$ to a cell, the only permissible motion is a $\theta - \phi$ circulation of matter in loops around the cell; the global crustal motion is inherently nonaxisymmetric. The footpoints of external magnetic field lines are embedded in the cell, so $\boldsymbol{v}_{\rm pl}$ causes a braiding of these; see Figure 1. $\bar{v}_{\rm pl}$ within a contiguous cluster of plastic cells plays two roles: it increases the average twist ψ of the associated coronal loop, $d\psi/dt = \bar{v}_{\rm pl}$, and is also taken to represent the rate of transfer of elastic to coronal energy $E_{\rm clus}$ for the cluster, so that

$$E_{\rm clus} = \psi(E_{\rm shallow} + E_{\rm deep}), \tag{7}$$

where $E_{\rm shallow}$ and $E_{\rm deep}$ are the sums of energy releases from all shallow and deep failures, respectively. The total coronal energy $E_{\rm corona}$ is then the sum of all $E_{\rm clus}$.

[3] Note that the inner crust will be solid for all these models; it first begins to melt for $T > 2 \times 10^9$ K.

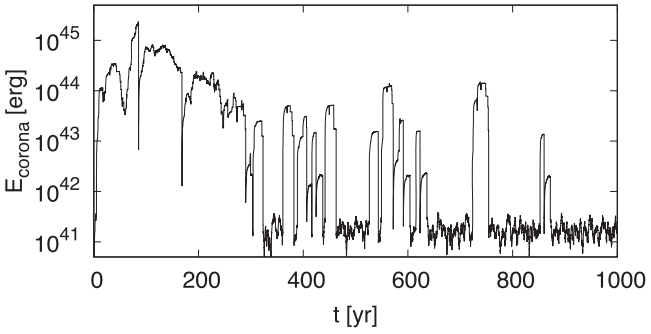

Figure 2. First 1000 yr of evolution, for $T_{amb,9} = 0.1$. E_{corona} is the total twist energy of all coronal loops.

Magnetar bursts are linked to magnetic reconnection in the corona (Lyutikov 2006), a complex process that is not well understood; any attempt to implement a detailed prescription risks introducing several new poorly constrained parameters, making the model harder to constrain or falsify afterwards. Instead we simply assume that when a plastic cluster ceases to exist, its remaining associated E_{clus} is emitted as a single burst. In the special case where at least one cluster's (average) twist reaches a peak value $\psi > 0.3$ rad, we impose a "high-twist" prescription where all coronal braids reconnect, ψ is reset to zero for each, and the total E_{corona} is ejected at once in a "giant flare."

3. Numerical Code

To avoid conceptual issues where the two footpoints of a coronal field line might both move in such a way that v_{pl} does not cause any increase in ψ, we assume one footpoint of every coronal field line is in the "active" northern hemisphere and the partner footpoint is in a "passive" southern hemisphere, releasing elastic energy but not driving the motion. Covering the northern hemisphere at a radius of 11.3 km (the outer boundary of the inner crust) requires ≈800 cells of 1 km^2 surface area; we also want a grid that is 4 times as long in ϕ as in θ (since $0 \leqslant \theta < \pi/2$, $0 \leqslant \phi < 2\pi$). We therefore choose a fiducial resolution of 14×56, i.e., 784 cells. For the top row of cells, identified with the pole, we set $\tau = 0$; those around the equator are assumed to be mirrored (for the purposes of counting numbers of plastic neighbors) with an unmodeled set of partner cells in the southern hemisphere. Periodic boundary conditions are imposed to identify the $\phi = 0$ and $\phi = 2\pi$ edges of the grid. The network of cells is evolved for 1000 yr with a C ++ code that tracks the formation, evolution, and extinction of plastic clusters, with a default time step of 0.01 yr. At the start of each simulation all cells are in the Hall phase, with stresses in the range $0.9 < \tau/\tau_{el} < 1.1$ randomly assigned to each cell. Thus, in this Letter the time $t = 0$ yr represents a mature magnetar's crust at age ∼1000 yr; the newborn crust is unstressed, so no seismic activity will occur at this stage. Differences in magnetic field strength and topology mean that some magnetars will reach this highly stressed state earlier than others, but are otherwise not likely to result in radically different behavior of the model.

4. Results

Figure 2 shows a representative example light curve from 1000 yr of evolution. The first high-twist "giant flare" event is seen at $t = 85$ yr. Figure 3 shows the crust's stress pattern

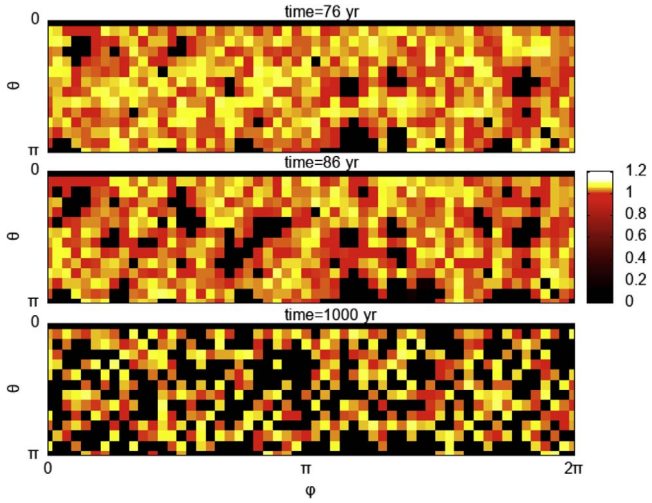

Figure 3. Snapshots of τ/τ_{el} (colorscale) across the northern hemisphere, just before (top) and after (middle) the first "giant flare," of 2×10^{45} erg, shown in the previous figure. τ/τ_{el} at 1000 yr (bottom) is also shown.

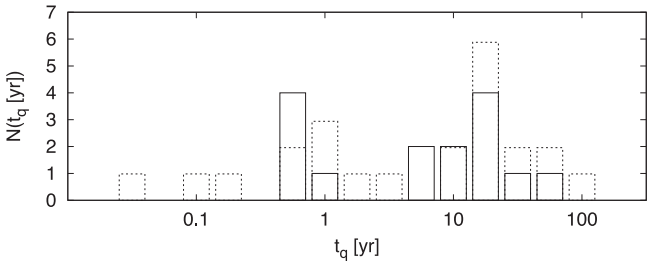

Figure 4. Number N of quiescent periods of duration t_q for two typical 1000 yr evolutions, at $T_{amb,9} = 0.05$ (solid bars) and $T_{amb,9} = 0.5$ (dashed bars).

before and after this event and demonstrates how every giant flare leaves behind extended patches of unstressed crust, thus reducing the chances of any future large-scale event occurring. The fractal pattern remaining after 1000 yr is characteristic of these simulations and is seen at higher resolutions too.

E_{corona} can be high for long periods without any individual loop developing high twist (although note that our simulations have no term for twist decay); in such a state the magnetar could be relatively quiet, but perhaps with a significantly nondipolar spindown rate (making estimates of the external field unreliable; Harding et al. 1999; Thompson et al. 2002). Long periods of "quiescence" (defined here as $E_{corona} < 10^{42}$ erg) punctuated by occasional intermediate events are seen, especially at later times. Figure 4 shows durations of these quiescent periods, for two representative runs with different T_{amb}. The distribution is roughly bimodal: our model magnetars go quiet for either a few months, or ∼10–30 yr. There is no correlation between the size of smaller events and the waiting time until the next one; though in the aftermath of a giant flare the model stars are—like real magnetars—often quieter.

The focus of this Letter is on understanding the crustal dynamics and transfer of energy to the corona, a widely accepted idea for high-energy magnetar bursts that is now also a leading model to explain (at least some) FRBs. Radio emission, however, is likely to require substantially lower levels of coronal twist than high-energy emission (Wadiasingh & Timokhin 2019), making it hard to reconcile the standard globally twisted magnetar corona model (e.g., Thompson et al. 2002) with recent observations of contemporaneous FRBs and

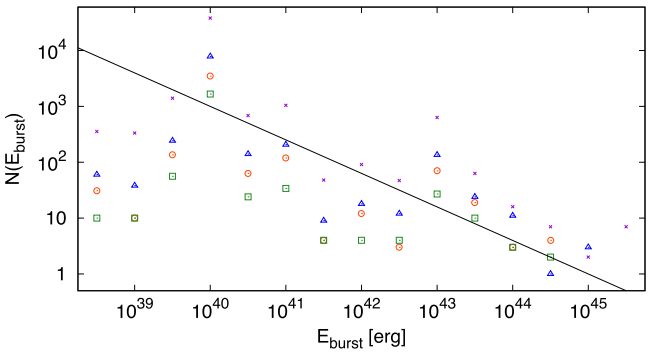

Figure 5. Number of bursts $N(E_{\rm burst})$ with energy $E_{\rm burst}$ over a 1000 yr simulation, in $\log(E_{\rm burst}) = 0.5$ bins, compared with a power-law relation of $\Gamma = 1.6$ (the line shown). Fixing a temperature $T_{\rm amb,9} = 0.5$, we explore the effect of cell size. Results for resolutions 14×56 (fiducial), 10×40, 20×80, and 44×176 are indicated with the circle, square, triangle, and cross points, respectively.

X-ray bursts from the magnetar SGR 1935+2154 (Bochenek et al. 2020; CHIME/FRB Collaboration et al. 2020; Mereghetti et al. 2020). By contrast, this Letter's model, where crustal failure leads to a network of more localized coronal braids with varying levels of twist, naturally allows for this.

While we cannot determine whether a given event from our evolutions will ultimately be seen as an X-ray burst or an FRB, since we do not study emission physics, we can still infer whether conditions in the corona are propitious for generation of a particular kind of radiation. From Figure 2 we see that for the first 300 yr the corona always contains a lot of twist energy, making FRB emission highly disfavored. Confirming observational results (Lin et al. 2020), we thus expect a classically active young magnetar to produce far more X-ray bursts than FRBs. Later on in our evolutions, energetic bursts of shorter duration occur, in between increasingly long periods of quiescence, and we thus anticipate—following Wadiasingh & Timokhin (2019)—that FRB emission will become more likely.

Figure 5 plots the burst energy distribution from 1000 yr of simulation, showing that burst numbers $N(E_{\rm burst})$ in the energy range $E_{\rm burst} = 10^{40}$–10^{45} erg broadly follow a Gutenberg–Richter (Gutenberg & Richter 1956) power law $dN/dE \propto E^{-\Gamma}$ independent of cell size. The total number of events does however increase with resolution, because there are more cells available to undergo elastic failure. Note that the evolution with 44×176 cells, 10 times the fiducial value, is shown as an extreme case; the other three resolutions are likely to be more realistic (recall Section 2.2). The infrequency of $E_{\rm burst} < 10^{40}$ erg events is an artifact of our model, which considers the inner crust only; lower-energy bursts are likely to involve the outer crust. Our model predicts that no magnetar will produce more than $\sim$10 giant flares over its first 1000 yr of maturity and—given the results of Figures 2 and 3—none at all thereafter.

Cellular automaton models, and many different kinds of astrophysical sources, generically exhibit power-law energy distributions with $\Gamma \approx 1.5$–2 (Aschwanden et al. 2016); in the fractal-diffusive model for cellular automata the key variable is the spatial dimension of the cell dynamics, with $\Gamma = 1.5$ predicted for 3D models (Aschwanden 2012). This is very close to the typical value $\Gamma = 1.6$ for magnetar X-ray bursts (Cheng et al. 1996; Göğüş et al. 1999, 2000; Gavriil et al. 2004), which is plotted in Figure 5 for comparison.

In corona-type cellular automata models, the cell rules encode an immediate diffusive redistribution of energy from one cell to its neighbors (Isliker et al. 2000) and lead to a tight N–E correlation (Lu & Hamilton 1991; Dănilă et al. 2015). Here the cell rules have the less direct effect of making energy release from a plastic cell's neighbors *more likely* rather than guaranteed, and as a result the burst statistics show more deviation from a simple power law. There is also an overrepresentation of 10^{40} and 10^{43} erg events (corresponding to a single cell's shallow or deep failure, respectively). Within the paradigm presented here, therefore, the degree of scatter of bursts from a power-law relation may encode valuable information about the nature of magnetar crustal failure.

5. Outlook

The model presented here was constructed based on theoretical considerations, and aims to be a faithful minimal representation of the salient physics of magnetar activity. Where possible, the model is quantitative: the crustal structure is calculated with a realistic equation of state, the elastic stress from a fit to molecular dynamics simulations, and the characteristic lengthscale for the cells taken from 3D magnetoelastic simulations. The details of how the crust fails are, however, unknown, which makes the use of somewhat ad hoc prescriptions inevitable. Nonetheless, we have performed extensive checks to confirm that the model's key results are robust to variation in cell size (see Figure 5), the expression for ν, and the critical value at which the transition between elastic and plastic regimes occurs. In particular, we have not attempted to "tune" any input quantities in order to better mimic the behavior of any particular magnetar. With this concrete model for crustal failure, however, we can now directly use information from magnetar bursts to constrain the model and the star's physics. For example, because even the largest events in our current model are relatively localized and weaker than the brightest known giant flare, this indicates the presence of an additional mechanism driving the propagation of crustal failure, e.g., a thermoplastic instability (Beloborodov & Levin 2014); this may be manifested observationally as deviations from the power law for weaker bursts. The detection of a giant flare with energy $\gtrsim 10^{47}$ erg would point to the involvement of core magnetic field evolution.

With a temperature-dependent plastic viscosity, hotter crusts produce frequent bursts, but slightly cooler ones are needed to allow time for a large plastic cluster to form and potentially power a giant flare. If the crust is too cold, however, the sluggish plastic flow is more likely to lead to long-lived multipolar coronal fields or nondipole spindown than outbursts. It will also be easier to observe FRBs from cooler crusts, since the more sparsely distributed coronal loops will not significantly inhibit radio emission (Suvorov & Kokkotas 2019; Wadiasingh & Timokhin 2019).

Very young and very old magnetars are not expected to produce giant flares: the former because large regions of high stress have not yet developed; the latter because numerous previous events have produced a fractal low-stress region that inhibits further large-scale failure.

Magnetar activity is often linked directly to the evolution of the star's toroidal $\boldsymbol{B}$, and although results of such simulations also inform our choice of cell geometry, our focus is instead on the distribution of evolving elastic stress in the crust. This evolution is driven by the changing $\boldsymbol{B}$, but is insensible to its

quantitative features. It is not obvious whether activity driven by an intense *poloidal* $\boldsymbol{B}$ would be noticeably different within our paradigm; perhaps it would lead to a different natural cell geometry. Any other source of stress could also, in principle, drive seismic activity, whether or not it then leads to characteristic magnetar behavior. The most obvious example would be stresses developing through spindown; in this case both the cell geometry and the evolution equations would need to be revised.

The crust is the éminence grise of magnetars: it powers their activity, but in a way that is difficult to discern from observations, which essentially "see" only the corona. The goal of this work is to provide a framework to compare observations directly with theory, and so to probe the crust's poorly understood mechanical properties.

It is a pleasure to thank Ersin Göğüş, George Younes, and Zorawar Wadiasingh for many stimulating discussions related to this work.

References

Andrade, E. D. C. 1934, London, Edinburgh, Dublin Phil. Mag. J. Sci., 17, 497
Aschwanden, M. J. 2012, A&A, 539, A2
Aschwanden, M. J., Crosby, N. B., Dimitropoulou, M., et al. 2016, SSRv, 198, 47
Bak, P., Christensen, K., Danon, L., & Scanlon, T. 2002, PhRvL, 88, 178501
Bak, P., Tang, C., & Wiesenfeld, K. 1988, PhRvA, 38, 364
Beloborodov, A. M., & Levin, Y. 2014, ApJL, 794, L24
Beloborodov, A. M., & Li, X. 2016, ApJ, 833, 261
Beniamini, P., Wadiasingh, Z., Hare, J., et al. 2023, MNRAS, 520, 1872
Berlekamp, E. R., Conway, J. H., & Guy, R. K. 2004, Winning Ways for your Mathematical Plays, Vol. 4 (Natick, MA: AK Peters/CRC Press)
Bochenek, C. D., Ravi, V., Belov, K. V., et al. 2020, Natur, 587, 59
Burns, E., Svinkin, D., Hurley, K., et al. 2021, ApJL, 907, L28
Caleb, M., Heywood, I., Rajwade, K., et al. 2022, NatAs, 6, 828
Cheng, B., Epstein, R. I., Guyer, R. A., & Young, A. C. 1996, Natur, 382, 518
CHIME/FRB Collaboration, Andersen, B. C., Bandura, K. M., et al. 2020, Natur, 587, 54
Chugunov, A. I., & Horowitz, C. J. 2010, MNRAS, 407, L54
Dehman, C., Viganò, D., & Rea, N. 2020, ApJL, 902, L32
Drossel, B., & Schwabl, F. 1992, PhRvL, 69, 1629
Dănilă, B., Harko, T., & Mocanu, G. 2015, MNRAS, 453, 2982
Gavriil, F. P., Kaspi, V. M., & Woods, P. M. 2004, ApJ, 607, 959
Gnedin, O. Y., Yakovlev, D. G., & Potekhin, A. Y. 2001, MNRAS, 324, 725
Göğüş, E., Woods, P. M., & Kouveliotou, C. 2000, ApJL, 532, L121
Göğüş, E, Woods, P. M., Kouveliotou, C., et al. 1999, ApJL, 526, L93
Gourgouliatos, K. N., De Grandis, D., & Igoshev, A. 2022, Symm, 14, 130
Gourgouliatos, K. N., & Lander, S. K. 2021, MNRAS, 506, 3578
Gourgouliatos, K. N., Wood, T. S., & Hollerbach, R. 2016, PNAS, 113, 3944
Gutenberg, B., & Richter, C. F. 1956, BuSSA, 46, 105
Harding, A. K., Contopoulos, I., & Kazanas, D. 1999, ApJL, 525, L125
Ho, W. C. G., Glampedakis, K., & Andersson, N. 2012, MNRAS, 422, 2632
Horowitz, C. J., & Kadau, K. 2009, PhRvL, 102, 191102
Hurley-Walker, N., Zhang, X., Bahramian, A., et al. 2022, Natur, 601, 526
Igoshev, A. P., Gourgouliatos, K. N., Hollerbach, R., & Wood, T. S. 2021, ApJ, 909, 101
Isliker, H., Anastasiadis, A., & Vlahos, L. 2000, A&A, 363, 1134
Jones, P. B. 2003, ApJ, 595, 342
Kaspi, V. M., & Beloborodov, A. M. 2017, ARA&A, 55, 261
Katz, J. I. 1986, JGR, 91, 10412
Kojima, Y., Kisaka, S., & Fujisawa, K. 2021, MNRAS, 502, 2097
Lander, S. K. 2016, ApJL, 824, L21
Lander, S. K., Andersson, N., Antonopoulou, D., & Watts, A. L. 2015, MNRAS, 449, 2047
Lander, S. K., & Gourgouliatos, K. N. 2019, MNRAS, 486, 4130
Li, C. K., Lin, L., Xiong, S. L., et al. 2021, NatAs, 5, 378
Li, X., Levin, Y., & Beloborodov, A. M. 2016, ApJ, 833, 189
Lin, L., Zhang, C. F., Wang, P., et al. 2020, Natur, 587, 63
Lu, E. T., & Hamilton, R. J. 1991, ApJL, 380, L89
Lyutikov, M. 2006, MNRAS, 367, 1594
Mereghetti, S., Savchenko, V., Ferrigno, C., et al. 2020, ApJL, 898, L29
Palmer, D. M. 1999, ApJL, 512, L113
Palmer, D. M., Barthelmy, S., Gehrels, N., et al. 2005, Natur, 434, 1107
Perna, R., & Pons, J. A. 2011, ApJL, 727, L51
Pons, J. A., & Viganò, D. 2019, LRCA, 5, 3
Ridnaia, A., Svinkin, D., Frederiks, D., et al. 2021, NatAs, 5, 372
Ruderman, M. 1991, ApJ, 382, 587
Scholz, P., & Kaspi, V. M. 2011, ApJ, 739, 94
Suvorov, A. G., & Kokkotas, K. D. 2019, MNRAS, 488, 5887
Thompson, C., & Duncan, R. C. 1995, MNRAS, 275, 255
Thompson, C., Lyutikov, M., & Kulkarni, S. R. 2002, ApJ, 574, 332
Thompson, C., Yang, H., & Ortiz, N. 2017, ApJ, 841, 54
Turolla, R., Zane, S., & Watts, A. L. 2015, RPPh, 78, 116901
Von Neumann, J., & Burks, A. W. 1966, ITNN, 5, 3
Wadiasingh, Z., & Timokhin, A. 2019, ApJ, 879, 4
Wei, J.-J., Wu, X.-F., & Dai, Z.-G. 2021, ApJ, 920, 153
Younes, G., Güver, T., Kouveliotou, C., et al. 2020, ApJL, 904, L21
Younes, G., Lander, S. K., Baring, M. G., et al. 2022, ApJL, 924, L27